Recycle Continuous-Flow Electrophoresis: Zero-Diffusion Theory

Recycle continuous-flow electrophoresis (RCFE) is a modification of Hannig's thin-film CFE device in which eluant is continuously recycled to the chamber inlet. Shifting the recycled eluent laterally a specific distance prior to reinjection enables the RCFE to separate any two solutes to arbitrary purity. This paper studies solute transport in an idealized RCFE in the absence of diffusion. The model is solved analytically by means of a two-sided Laplace transform. Three distinct types of solute distribution are found, and guidelines for construction and operation of an RCFE are derived.

William A. Gobie, Cornelius F. Ivory
Department of Chemical Engineering
Washington State University
Pullman, WA 99164

Introduction

The success of electrophoresis as the underlying principle in a variety of analytical- and preparative-scale separation techniques inspired development of larger scale continuous apparatuses as early as 1939 (Philpot, 1940). The current rapid development of commercial biotechnology has rekindled interest in large-scale zone electrophoresis for downstream processing. Apparatuses proposed or demonstrated include the velocity-gradient stabilized Biostream or Philpot-Harwell apparatus (Mattock et al., 1980), the continuous rotating annular electrophoresis (CRAE) column (Yoshisato et al., 1986), "thick film" continuous-flow electrophoresis in space, and the recycle continuous-flow electrophoresis apparatus considered in this paper.

Our recycle continuous-flow electrophoresis (RCFE) apparatus is based on Hannig's thin-film continuous-flow electrophoresis (CFE) apparatus, developed some thirty years ago (Svensson and Brattsten, 1949; Grassmann, 1950; Grassmann and Hannig, 1953; Barrolier et al., 1958; Hannig, 1969). In CFE, sketched in Figure 1, a laminar curtain of buffered carrier fluid passes through a broad, thin chamber. The feed mixture is introduced into the curtain as a thin stream. The mobile components electrophorese laterally as they pass between the electrodes and are collected in separate fractions at the chamber exit. Cooling jackets (not shown) external to the broad transverse walls remove Joule heat dissipated by the electric current.

This apparatus design requires a compromise between throughput and resolving power. Throughput increases with the transverse gap width, but several factors degrade resolution as gap width increases, and there are fundamental limits to gap width imposed by cooling considerations. Cooling efficiency and viscous stress decrease as the gap is widened, making the liquid film vulnerable to thermally induced buoyancy instabilities (Saville and Ostrach, 1978). Consequently the transverse dimension of terrestrial CFE chambers has been limited to 0.5–1 mm.

Solute bands disperse laterally by "crescent formation" (Strickler, 1967), which results from the superposition of two convective effects. First, the solute's residence time varies with transverse position due to the curtain's laminar velocity profile. Solute near a transverse wall remains in the electric field longer than solute near the centerline and experiences a greater electrophoretic deflection. Second, electroosmotic flow along the transverse walls sets up a recirculating lateral flow, dispersing the solute convectively. It is possible to influence crescent formation by coating the chamber walls with a material of suitable zeta potential (Strickler and Sacks, 1973), but it can be eliminated entirely for only one component of a mixture and is difficult to control. Crescent formation is mitigated in practice by injecting feed through a narrow tube, of diameter 20–30% of the gap width, centered in the gap (Hannig, 1982). This restricts solute to the portion of the flow field having the most uniform velocity. Compared with a square feed port spanning the gap, throughput is reduced by roughly $O(10)$.

The modifications that transform CFE into RCFE are primarily intended to address the problem of crescent formation, but also have important implications for hydrodynamic stability because they allow operation at reduced power input.

RCFE is illustrated in Figure 2a. Recycle streams connect the exit and entrance planes so that the curtain cycles repeatedly through the electrophoresis chamber. The recycle streams are connected to shift the curtain laterally the distance s on each cycle. Feed is injected directly into a recycled stream, although this will produce a slightly nonuniform velocity field. Should this prove too disruptive, solvent could be removed from the

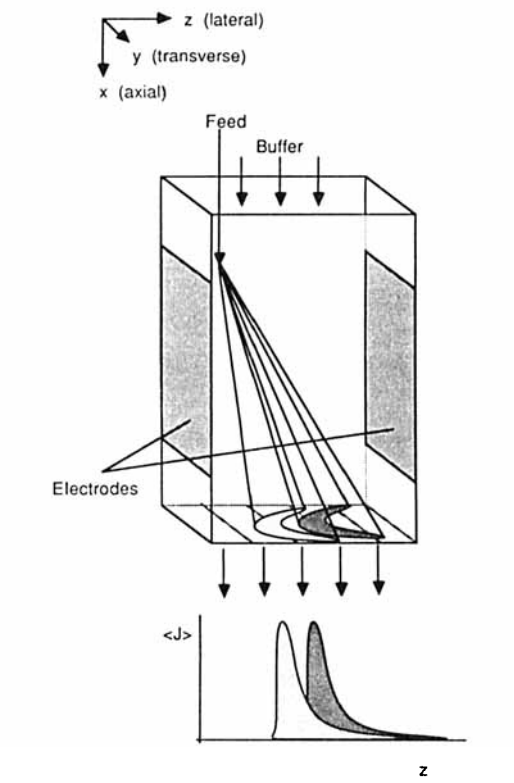

Figure 1. Classic thin-film CFE.

As buffer curtain carries feed mixture through electrophoresis chamber, mobile species migrate laterally, forming electrophoretic spectrum at chamber exit. Residence time and electroosmotic effects distort solute band cross sections into crescents, producing overlapping flux distributions $\langle J \rangle$ at the exit

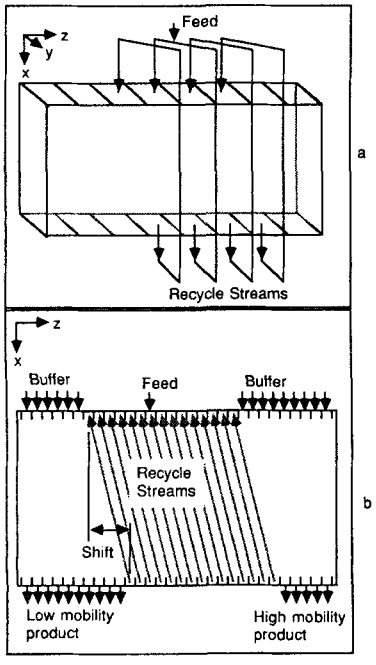

Figure 2. Recycle CFE.

a. Each exit port in recycle section is connected to an inlet port by a recycle stream; here the buffer curtain is shifted left one port on each cycle

b. In a complete RCFE apparatus buffer is injected through unconnected inlet ports on either side of recycle section, and purified products are withdrawn through exit ports flanking the recycle section

recycle stream by ultrafiltration. The quantity of solvent removed also influences the concentration at which products may be recovered.

Figure 2b depicts the entire RCFE flow scheme. Within the recycle section, exit and inlet ports are connected by recycle streams. A uniform velocity field is maintained by injecting carrier fluid through the extra inlet ports, while purified products are withdrawn through the exit ports flanking the recycle section. All streams have identical flow rates.

Purified products are found at opposite sides of the recycle section because the shift imparts a lateral velocity to the curtain. If s is properly chosen, this lateral flow will oppose the solutes' electrophoretic migration and wash the slower solute downstream while the faster solute continues to migrate upstream.

In RCFE, crescent formation occurs just as in conventional CFE, but its effects are mitigated by recycle because mixing within each recycle stream homogenizes the concentration within each stream. The solute distribution impinging on an exit port is thus averaged and redistributed uniformly over the corresponding inlet port. The solute will appear to have a large transverse dispersion coefficient. This produces an interesting manifestation of Taylor dispersion, in which the mixing and dispersing processes occur in separate parts of the apparatus, rather than simultaneously as in Taylor's experiments (Taylor, 1953). This effect is fundamental to RCFE operation: When observed over many cycles, the solute band will appear to disperse diffusively rather than convectively. If n is the number of cycles a solute moiety has made, then its dispersion will be proportional to $\sqrt{n}$, while its electrophoretic displacement will be proportional to n (Gobie, 1987). Thus the rate at which two solutes separate exceeds the rate at which dispersion remixes them, and they can be separated to any desired purity if n is large enough.

Experiments in our laboratory with an RCFE apparatus having 50 inlet and outlet ports have validated the foregoing arguments. The results are in qualitative agreement with previously published models (Gobie et al., 1985) and with the model presented below. These results have been presented in a separate report (Gobie and Ivory, 1987).

Theory

There are many different approaches one can take to modeling RCFE (Gobie et al., 1985; Gobie, 1987). Here we develop a simple yet rigorous model that reveals the fundamental behavior of RCFE and its limiting ideal performance.

We assume that the recycle section is infinitely wide and that the recycle ports have infinitesimal lateral width, i.e., that they are continuous. This frees us from specifying mathematically how the purified solute is collected and simplifies treatment of the recycle streams. Infinitesimally wide ports in fact represent a desirable physical limit in which dispersion arises solely from crescent formation.

We further assume that phenomenological coefficients are constant, and that the electric field is uniform.

Solute transport within the chamber is described by the continuity equation,

$$u_0[1 - (y/B)^2]\frac{\partial C}{\partial x} + \left[u_e + u_w - \frac{3}{2}u_w(1 - (y/B)^2)\right]\frac{\partial C}{\partial z} = D\nabla^2 C \quad (1)$$

where u_0 is the centerline velocity, $2B$ is the gap width, u_E is the electrophoretic velocity, and u_w is the electroosmotic velocity at the wall. The electrophoretic velocities are defined as the products of the electric potential gradient and a characteristic mobility.

Transverse and lateral boundary conditions are

$$\frac{\partial C}{\partial y} = 0 \text{ at } y = \pm B \tag{2}$$

$$\frac{\partial C}{\partial z} \to 0 \text{ as } |z| \to \infty \tag{3}$$

The lateral condition, Eq. 3, is deduced from the fact that the ratio of solute to solvent is constant because both are introduced at constant rates in the feed and neither is removed from the apparatus. Sufficiently far from the feed, dispersion smooths out any variation in concentration.

The axial boundary condition expresses the operation of the recycle streams. We assume that there are no axial, lateral, or transverse gradients at an inlet port. Supposing that an inlet port with lateral coordinate z is connected to an exit port at $z - s$, the convective flux through the inlet port is the product of axial velocity and the mean concentration entering the exit port:

$$J_x(0, y, z) = \frac{u_x(y)}{\langle u_x(y)\rangle} \int_{-B}^{B} J_x(L, y, z - s)\, dy + C_0 u_x(y)\delta(z) \tag{4}$$

L is the length of the chamber, s is the recycle shift, and C_0 is the feed concentration. Feed injection is modeled as an impulse located at the origin, and we assume it does not alter the velocity field.

Far-field concentration

Before proceeding with the microscopic model, it is interesting to pursue the implications of the observations made in connection with the boundary condition, Eq. 3. Consider a macroscopic mass balance on a control volume as indicated in Figure 3. The volume extends the entire length of the chamber, and from the point z_0 leftward to $-\infty$. It includes the feed. Assume that the electric field, curtain velocity, and shift have been selected so that the solute has a net positive lateral velocity. Concentration therefore falls to zero for negative values of z, and since the ratio of solute to solvent in the entire chamber is constant, concentration must approach a constant nonzero far-field value for positive values of z. We can obtain this value with a macroscopic mass balance:

$$\int_{-B}^{B}\int_{-\infty}^{z_0} J_x(0, y, z)\, dzdy = \int_{-B}^{B}\int_{-\infty}^{z_0} J_x(L, y, z)\, dzdy + \int_{-B}^{B}\int_{0}^{L} J_z(x, y, z_0)\, dxdy \tag{5}$$

The integral on the lefthand side of Eq. 5 represents solute entering the control volume along the inlet plane. The terms on the righthand side represent solute leaving the volume through the exit plane and through the surface at z_0. After replacing the integrand on the lefthand side with the recycle boundary condition, Eq. 4, and breaking the new integral into an integral over

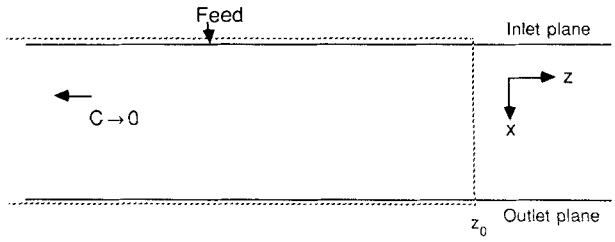

Figure 3. Control volume used for deriving far-field concentration.

$[-\infty, z_0]$ and an integral over $[z_0, z_0 - s]$, we obtain

$$\int_{-B}^{B}\int_{z_0}^{z_0 - s} J_x(L, y, z)\, dzdy + 2B^2 C_0 \langle u_x(y)\rangle = \int_{-B}^{B}\int_{0}^{L} J_z(x, y, z_0)\, dxdy \tag{6}$$

Now let the point z_0 be far enough from the feed that dispersive forces average out all variation in concentration. The fluxes becomes products of concentration and mean velocity, yielding

$$C^{FF} = \frac{C}{C_0} = \frac{\langle u_x\rangle}{\frac{L}{B}\langle u_z\rangle + \frac{s}{B}\langle u_x\rangle} = \frac{1}{\frac{L}{B}\frac{\langle u_z\rangle}{\langle u_x\rangle} + \frac{s}{B}} \tag{7}$$

Equation 7 defines the far-field concentration. The center form shows it is the ratio of the solute's axial to lateral velocity, i.e., the concentration ratio at which the axial and lateral convective fluxes balance. From the extreme righthand side, this is equivalent to the reciprocal of the solute's mean displacement after a single transit of the chamber and recycle streams. Both forms imply that the sign of C^{FF} indicates on which side of the feed we will find the far-field concentration.

The far-field concentration is plotted in Figure 4 for a particular choice of chamber length L/B, and shift s/B, as a function of scaled electrophoretic velocity, $\langle u_z\rangle/\langle u_x\rangle = \mu E/\langle u_x\rangle$. For an electric field less than the cricial value $E_c = -s\langle u_x\rangle/(L_\mu)$, all the solute eventually winds up on the left of the feed. As E approaches E_c the far-field flux increases without bound. When

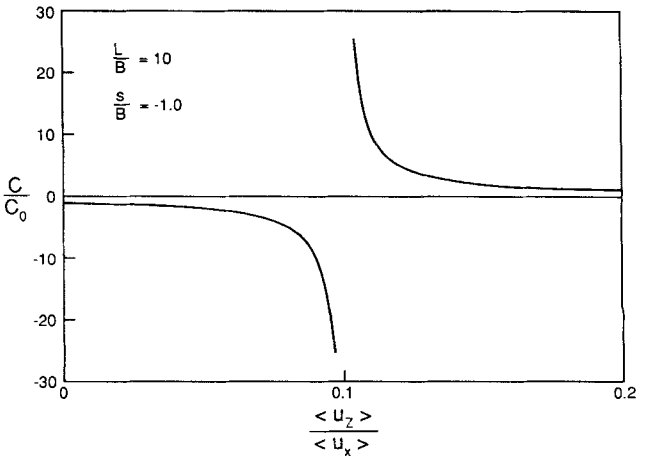

Figure 4. Far-field concentration as a function of electrophoretic velocity.

E exceeds E_c the solute's mean displacement on each cycle is positive, and the far-field flux occurs to the right of the feed. Further increasing E diminishes the far-field concentration.

C^{FF} becomes singular when $E = E_c$ because at this value of E convective removal of solute from the control volume ceases. This result indicates that RCFE can concentrate solutes above their feed concentrations. Whether the material can be withdrawn from the apparatus at this concentration is another matter, which we will consider further in the discussion.

Zero-diffusion model

The general model, Eqs. 1–4, is extremely difficult to solve because the continuity equation is nonself-adjoint. It has been solved for the case of solute making a single transit of the electrophoresis chamber (Gobie, 1987), but the solution is too complex to aid us here. To simplify the analysis, we consider the limit of zero diffusion, $D = 0$. Choosing the dimensionless variables given in Table 1, the model becomes

$$(1-\eta^2)\frac{\partial C^*}{\partial \xi} + \left[\epsilon + \nu - \frac{3}{2}\nu(1-\eta^2)\right]\frac{\partial C^*}{\partial \zeta} = 0 \tag{8}$$

$$C^*(0,\eta,\zeta) = \frac{3}{2}\int_0^1 (1-\eta^2)C^*(\lambda,\eta,\zeta-\sigma)\,d\eta + \delta(\zeta) \tag{9}$$

$$\frac{\partial C^*}{\partial \zeta} \to 0 \text{ as } |\zeta| \to \infty \tag{10}$$

In scaling Eq. 4 one obtains an integral over $[-1, 1]$. This interval has been changed to $[0, 1]$ in Eq. 9 since the integrand is an even function of η.

Transverse boundary conditions are no longer required. Equation 8 is readily solved by characteristics to give

$$C^*(\xi,\eta,\zeta) = C^*\left[0,\eta,\zeta - \xi\left(\frac{\epsilon+\nu}{1-\eta^2} - \frac{3}{2}\nu\right)\right] \tag{11}$$

Equation 8 is the basis of numerous models of conventional CFE, due to its simplicity and the fact that for most species separated by electrophoresis the Peclet number is $O(10^4)$ at least. Strickler (1967) used the solution, Eq. 11, to estimate the contribution to dispersion due to crescent formation. Vaughn (1983), Saville and Ostrach (1978), and Gionnovario et al. (1978) constructed models of solute transport incorporating temperature-dependent transport properties and employed a computer to solve Eq. 8 by ray-tracing.

When Eq. 11 is substituted into the recycle boundary condition, Eq. 9, we obtain an integral equation,

$$C^*(\zeta) = \frac{3}{2}\int_0^1 (1-\eta^2) \cdot C^*\left[\zeta - \sigma - \lambda\left(\frac{\epsilon+\nu}{1-\eta^2} - \frac{3}{2}\nu\right)\right]d\eta + \delta(\zeta) \tag{12}$$

Concentration at the inlet plane is independent of η because of mixing in the recycle streams. Since only the concentration at the inlet plane appears in Eq. 12, the first two arguments of C^* have been dropped. In the remainder of this paper $C^*(\zeta)$ stands for concentration at the chamber inlet. Concentration elsewhere in the chamber can be found using Eq. 11.

Table 1. Scaling and Dimensionless Parameters Used in Zero-Diffusion Model

$\xi = x/B$	$\gamma = \sigma + \lambda(\epsilon - \nu/2)$
$\epsilon = u_E/u_0$	$\zeta = z/B$
$\lambda = L/B$	$\sigma = s/B$
$\eta = y/B$	$\beta = \lambda(\epsilon + \nu)$
$\nu = u_w/u_0$	$C^* = C/C_0$

Equation 12 can be shown to be a Volterra equation of the second kind. However, it is convenient to leave it in its present form and apply a two-sided Laplace transform (van der Pol and Bremmer, 1955).

$$\bar{C}(p) = \int_{-\infty}^{\infty} C^*(\zeta)\, e^{-p\zeta}\, d\zeta \tag{13}$$

The two-sided Laplace transform shares most of the operational properties of the better known one-sided transform. It is well suited to handling the recycle shift in Eq. 12 through the familiar shift rule, $L[f(z-s)] = L[f(z)]e^{-ps}$. The two-sided transform is easier to invert than the more commonly used exponential Fourier transform when the transform involves a rather rare transcendental funciton. And whereas the Fourier transform would require that $C^*(\zeta)$ decay to zeros as $|\zeta| \to 0$, the Laplace transform is less strict, requiring $C^*(\zeta)$ to be of exponential order. $C^*(\zeta)$ clearly meets this requirement by the condition of Eq. 3.

Applying the Laplace transform to Eq. 12 removes η from the argument of C^*, so that one easily finds the Laplace transform of the solute distribution at the chamber inlet to be

$$\bar{C}(p) = \frac{1}{1 - \frac{3}{4}e^{-p(\sigma - 3/2\lambda\nu)}\int_0^1 (1-\eta^2)\exp\left[-\frac{p\lambda(\epsilon+\nu)}{1-\eta^2}\right]d\eta} \tag{14}$$

Now comes the problem of inverting this Laplace transform. We give two inversions, one useful for qualitative study of the solute distribution in RCFE, and a second that can be used for computations.

Qualitative inversion

The analytic continuation of the integral appearing in the denominator of Eq. 14 is a Kummer function of the second kind (Abramowitz and Stegun, 1964; Lebedev, 1972). Using the Kummer function's asymptotic expansion in terms of a hypergeometric function and the Taylor series

$$\frac{1}{1-x} = 1 + x + x^2 + x^3 + \cdots \tag{15}$$

we can obtain (van der Pol and Bremmer, 1955) the "qualitative inversion"

$$C^*(\zeta) = \delta(\zeta) + f(\zeta) + \int_{-\infty}^{\infty} f(u)\, f(\zeta - u)\, du + \int_{-\infty}^{\infty}\int_{\infty}^{\infty} f(v)\, f(u - v)\, f(\zeta - u - v)\, du\, dv + \cdots \tag{16}$$

where

$$f(\zeta) = \frac{3}{4}\beta^{-1}\left(1 + \frac{\zeta - \gamma}{\beta}\right)^{-5/2}\left(\frac{\zeta - \gamma}{\beta}\right)^{-1/2} H\left(\frac{\zeta - \gamma}{\beta}\right) \qquad (17)$$

Depending on γ and β, the Heaviside function $H(\cdot)$ in Eq. 17 will introduce ζ into either the upper or lower limits of integration in Eq. 16, so Eq. 16 has the classic form for the solution of a Volterra equation. As is typical of such a solution, a causal relationship exists between successive terms. The first term is the feed, the second is the band's distribution after passing once through the chamber and recycle streams, the third is the band's distribution after a second cycle, and so on. The nth term represents the band's distribution after $(n - 1)$ cycles. Their superposition gives the overall solute distribution.

The function $f(\zeta)$ in Eq. 17 is the Green's function for this problem. From the physical interpretation of Eq. 16, setting $\sigma = 0$ in Eq. 17 gives the solute distribution that would be observed at the exit plane of a conventional CFE apparatus operating under zero-diffusion conditions with a line-impulse feed distribution. This expression is used below to compare separation in RCFE and CFE.

The groups γ and β, defined in Table 1, play prominent roles in this solution. Their physical interpretation is the following. Because the velocity $(\epsilon - \nu/2)$ occurs at the chamber centerline, γ is the displacement of the solute band's head or leading edge on each cycle, Figure 5. Since $\gamma + \beta/2 = \sigma + 3/2\,\lambda\epsilon$, β determines the displacement of the band's head from its mean, and therefore measures the intensity of dispersion (crescent formation). Equation 17 shows that β sets the lateral scale of the distribution, thus the distribution scales with the intensity of crescent formation.

Studying the trajectories of the solute band's mean and head reveals that three distinct types of overall solute distribution are possible under zero-diffusion conditions. Assuming $\beta > 0$:

Case 1, $\gamma > 0$, $\gamma + \beta/2 > 0$. This situation is illustrated in Figures 5 and 6a. The head and mean of the band travel right on each cycle. Since the solute's lateral velocity is positive, the far-field concentration occurs on the right. The left edge of the distribution will be quite sharp because it is formed by the band on its first pass. No solute will be found to the left of the feed.

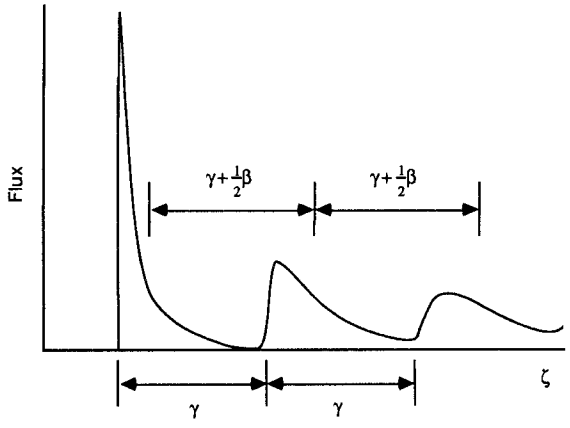

Figure 5. Physical interpretation of groups γ and β.
γ is distance band's head advances on each cycle
β measures intensity of crescent formation
$\gamma + \beta/2$ is distance band's mean advances on each cycle

Case 2, $\gamma < 0$, $\gamma + \beta/2 > 0$. This case is shown in Figure 6b. Solute is found on both sides of the feed because the head of the band is displaced to the left on each cycle. Because the solute's mean velocity is positive—i.e., the band's mean is displaced to the right on each cycle—all the solute crossing into the left half of the chamber is eventually sent back to the right half. The overall distribution falls gradually to zero on the left, and reaches the nonzero far-field value on the right.

Case 3, $\gamma < 0$, $\gamma + \beta/2 < 0$. See Figure 6c: the far-field concentration occurs on the left because now the solute has a negative net lateral velocity. The overall distribution has a long toe extending into the right half of the chamber because at infinite (and high) Peclet number the band has a long tail. These tails overlap to form the toe.

If $\beta < 0$ then we observe the mirror images of these cases.

Equation 17 is unsuitable for calculations due to the iterated convolutions, so we turn to the second method of inverting Eq. 14.

Quantitative inversion

If the integral in Eq. 14 is replaced with the exact expression for the Kummer function (Abramowitz and Stegun, 1964), the Laplace transform becomes

$$\bar{C}(p) = \frac{1}{1 - \frac{3}{4}\pi^{1/2}(p\beta)^2 e^{-p\gamma}U(\frac{5}{2}, 3, p\beta)} \qquad (18)$$

$U(\cdot, \cdot, \cdot)$ is the Kummer function of the second kind.

Equation 18 is inverted by using the general inversion formula for the Laplace transform,

$$C(\zeta) = \frac{1}{2\pi i}\int_{a-i\infty}^{a+i\infty} \bar{C}(p)e^{-p\zeta}\,dp \qquad (19)$$

The contour integration involved in evaluating Eq. 19 is complicated by the Kummer function's branch cut along the negative real axis. Details may be found elsewhere (Gobie, 1987). The result is summarized in Table 2. The quantities R, F, and I are defined as

$$R = \sum_n \frac{e^{r_n\zeta}}{\frac{dD}{dp}(r_n)} \qquad (20a)$$

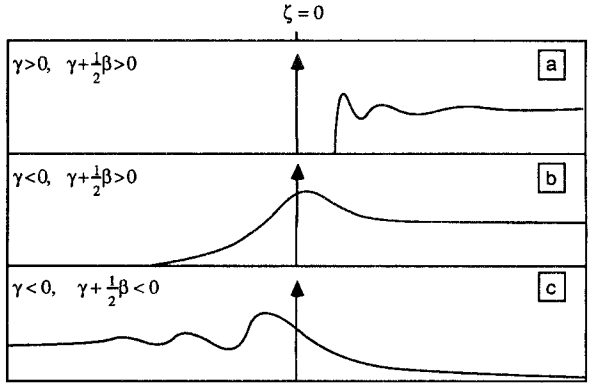

Figure 6. The three types of solute distribution predicted by the qualitative inversion.

Table 2. Quantitative Inversion of Zero-Diffusion Model

Case		$\zeta > 0$	$\zeta < 0$
1	$\gamma > 0$ $\gamma + \beta/2 > 0$	$C(\zeta) = R + F + I$	$C = 0$
2	$\gamma < 0$ $\gamma + \beta/2 > 0$	$C(\zeta) = F + I$	$C(\zeta) = -R$
3	$\gamma < 0$ $\gamma + \beta/2 < 0$	$C(\zeta) = I$	$C(\zeta) = -R - F$

R, F, I, defined in Eq. 20

$$F = \frac{1}{\sigma + \frac{3}{2}\lambda\epsilon} \tag{20b}$$

$$I = \frac{1}{\pi}\int_0^\infty \mathrm{Im}[\bar{C}(-p)]\, e^{-p\zeta}\, dp \tag{20c}$$

The numbers r_n appearing in Eq. 20a are the poles of the Laplace transform, the zeros of

$$D(p) = 1 - \tfrac{3}{4}\pi^{1/2}(p\beta)^2 e^{-p\gamma} U(\tfrac{5}{2}, 3, p\beta) \tag{21}$$

Numerical investigation reveals that poles are only found in one half-plane: in the left half-plane for a case 1 distribution, in the right half-plane for cases 2 and 3. There are an infinite number of complex conjugate poles, and for a case 2 distribution there is also a single real pole. The origin is a zero of Eq. 21, but its contribution is explicitly handled as the quantity F, Eq. 20b.

The integral defining the quantity I, Eq. 20c, is itself a one-sided Laplace transform, which we evaluate numerically by transforming the integral to the interval $(-1, 1)$ and integrating with an adaptive quadrature algorithm employing open interval formulas.

Results

Figure 7 illustrates the effect of the scale factor β for a case 1 distribution. In these and all subsequent figures the impulse function simulating feed injection at $\zeta = 0$ has been suppressed. The nth peak corresponds to the solute band's nth cycle. The band broadens as it cycles through the apparatus, eventually overlapping itself to such a degree that the individual passes are indistinguishable. As β is reduced the solute distribution compresses toward $\zeta = 0$ and the far-field flux increases.

Figure 8 samples each of the three solute distributions by varying the shift. As the shift increases, the solute distribution first squeezes toward $\zeta = 0$, giving a sequence of distributions similar to that for β decreasing. But when γ changes sign, solute "spills over" into the left half of the chamber as shown in Figure 8b. The head of the solute band now moves leftward on each cycle. In Figure 8b the head can be distinguished clearly on its first two cycles. Since the band's mean moves right on each cycle, all the solute crossing into the left half of the chamber is eventually sent back to the right. As the shift is further increased the distribution stretches out along the negative ζ axis, and the far-field flux continues to increase. When the group $\gamma + \beta/2$ changes sign, the far-field flux switches to the negative ζ axis and begins to decrease in magnitude, and we see distributions like that in Figure 8c. Now both the band's head and mean

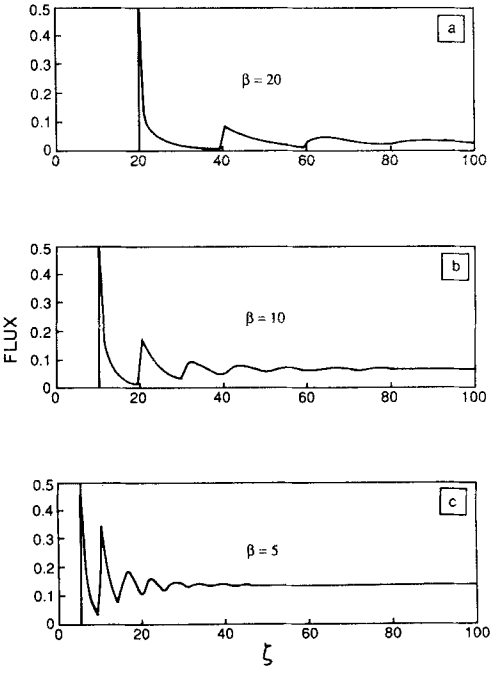

Figure 7. Effect of scale factor β.
For all cases, $\epsilon = 1, \nu = 0, \sigma = 0$. As scale factor is reduced, distributions remain qualitatively identical

move leftward on each cycle. Since the band's tail stretches out to the right, we still find solute in the right half of the chamber.

In Figure 9 we simulate separation of two solutes whose mobilities differ by 20%. Table 3 summarizes the conditions for this simulation. For comparative purposes, Figure 10 presents

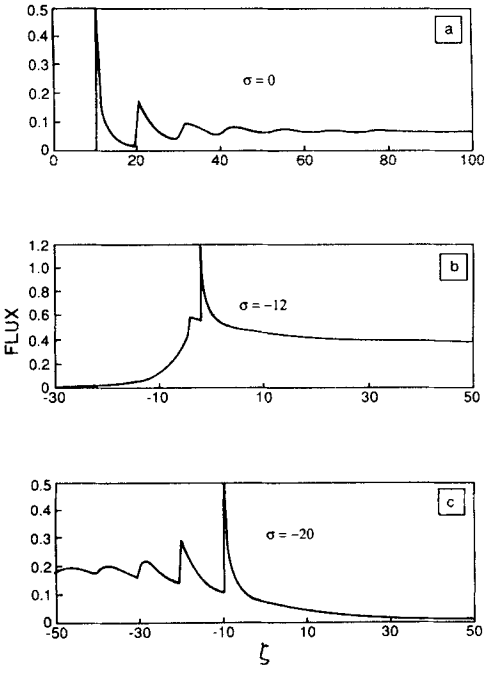

Figure 8. Effect of shift σ.
For all cases, $\epsilon = 1, \nu = 0, \lambda = 10$
As shift increases each of the different qualitative types of solute distribuiton is observed

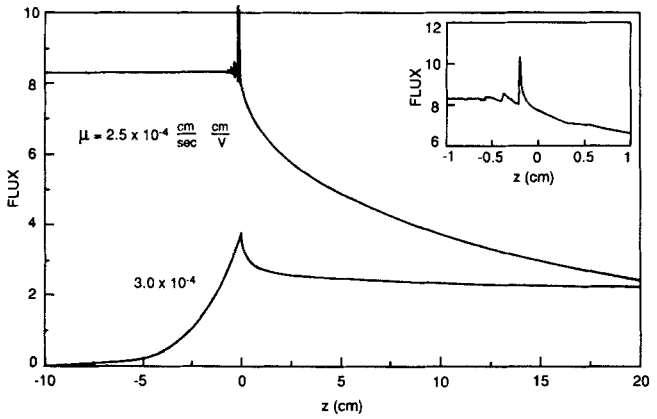

Figure 9. Simulated separation in RCFE of solutes differing by 20% in mobility.
Inset shows an expanded view of upper curve near $z = 0$

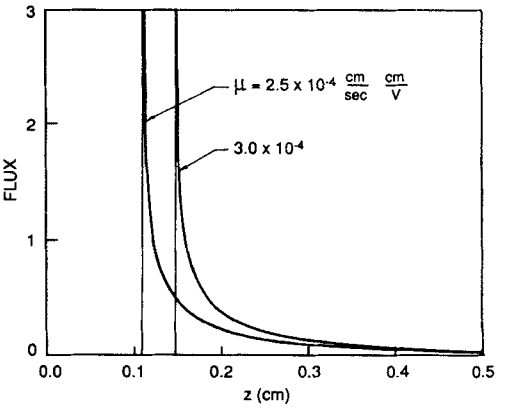

Figure 10. Simulated separation in conventional CFE of solutes differing by 20% in mobility.

the distributions that would be observed if this separation were attempted in conventional CFE, with feed injected all across the gap, as in RCFE. Whereas no useful separation occurs in CFE, RCFE purifies solute 2 within 10 cm of the feed port. To purify solute 1, either a considerably wider recycle section is required or (preferably) the device should be operated at different conditions.

Discussion

Operating conditions

The qualitative inversion provides useful guidelines for selecting operating conditions. Optimally, these should be selected so that the components of a binary feed exhibit distribution types 1 and 3. Then the leftward migrating component can be collected at high purity at any point left of the feed. The width of the recycle section required for the separation will depend entirely on the desired purity of the rightward migrating component. Purity increases rapidly with distance, since the leftward migrating component's tail has the asymptotic dependence ζ^{-3}.

The qualitative inversion shows that β sets the lateral scale of the distribution, and this is reflected in Figures 7 and 8 where concentration reaches its far-field values at a distance of 5–6β. Thus β provides a simple estimate of the relaxation distance on the side of the feed on which the far-field flux occurs.

In general, two solutes can be separated when the group $\sigma + \frac{3}{2}\lambda\epsilon$ has opposite sign for the two solutes. In practice one will be faced with choosing the optimal electric field strength, since the shift is difficult to change once the device is assembled. So to separate two species with mobilities $\mu_1 > \mu_2$, one must choose E within the range

$$-\frac{2}{3}\frac{\sigma u_0}{\lambda\mu_1} < E < \frac{2}{2}\frac{\sigma u_0}{\lambda\mu_2} \tag{22}$$

Table 3. Conditions for Separation Simulated in Figures 9 and 10

$B = 0.1$ cm	$\mu_1 = 3 \cdot 10^{-4}$ cm/s · cm/v
$u_0 = 0.5$ cm/s	$\mu_2 = 2.5 \cdot 10^{-4}$ cm/s · cm/v
$L = 16.$ cm	$\mu_w = 2.15 \cdot 10^{-4}$ cm/s · cm/v
$s = -0.3$ cm	$E = 24$ v/cm

Additionally, for ease of separation, one would like solute 1 to exhibit distribution type 1 and solute 2 distribution type 3. This gives the additional constraint

$$\frac{\sigma u_0}{\lambda(\mu_w/2 - \mu_1)} < E < \frac{\sigma u_0}{\lambda(\mu_w/2 - \mu_2)} \tag{23}$$

Constraint 22 must be met to obtain separation. Meeting constraint 23 is desirable, but this depends on the species being separated and the intensity of electroosmosis. For example, supposing that Eq. 22 gives the upper limit on E for a particular separation, and that Eq. 23 gives the lower limit, it is easy to find that for optimal separability,

$$\frac{2}{3}(\mu_1 - \mu_w/2) > \mu_2 \tag{24}$$

Thus, device dimensions play no role in determining whether one solute of a pair will form a type 1 distribution and the other a type 3 distribution. We may say that when inequality Eq. 24 is met the separation is easy in an RCFE apparatus and difficult otherwise.

If constraint 23 cannot be met, both solutes will be present on each side of the feed. Choice of E then depends crucially on the apparatus dimensions, for these will determine the trade-off between purity and yield of the more important solute. For high purity, one would like to choose E to maximize $|\sigma + \frac{3}{2}\lambda\epsilon|$ for the contaminating solute; however, this will simultaneously increase the relaxation distance of the other solute, possibly leading to loss of a portion of it if the recycle section is not wide enough.

The separation simulated in Figure 9 illustrates this trade-off. It satisfies the definition of a difficult separation. Constraint 22 requires 21 v/cm $< E <$ 25 v/cm. Within these limits constraint 23 cannot be met since it requires 31 v/cm $< E <$ 38 v/cm. Assuming that solute 1 is the contaminant, we attempt to minimize the lefthand relaxation distance of solute 1 by choosing $E = 24$ v/cm. From Figure 9, solute 2 could be recovered essentially pure beyond $z = -10$ cm, but a considerable fraction of it may be lost because its distribution's toe extends far into the right half of the chamber. Reducing E to shorten the toe will lengthen solute 1's toe, making it more difficult to purify solute 2.

Far-field concentration

When $\sigma + \frac{3}{2}\lambda\epsilon = 0$, the concentration everywhere in the chamber becomes infinite. Physically, this means that solute is introduced into any control volume containing the feed more quickly than it is removed. It can be shown that due to the mixing occuring during recycle, the solute will disperse laterally by Taylor dispersion, so that the standard deviation of the solute band will be proportional to $\sqrt{n}$, where n is the number of cycles the band has made (Gobie, 1987). When $\sigma + \frac{3}{2}\lambda\epsilon = 0$, this dispersion will be the only mechanism removing solute from the control volume. Since the amount of solute fed to the control volume grows linearly with time, concentration will increase until some other physical mechanism, such as precipitation, commences removing solute.

In an actual RCFE apparatus the ports' finite lateral width is an additional source of dispersion. But this will be Taylor-dispersive in nature, so the above argument holds for both actual and idealized RCFE devices.

Although the recycle section can concentrate a solute above its feed concentration, the concentration at which it can be withdrawn from the apparatus is fixed by mass conservation as $C/C_0 = F/Q$, where F is the volumetric feed rate and Q is the volumetric flow rate through a single recycle stream. The factors affecting F/Q depend upon the apparatus design and the choice of operating conditions, subjects better left to a separate paper.

In an actual RCFE apparatus, the division between the three types of solute distribtuion will not be clear-cut. Lateral dispersion introduced by the recycle ports will smear the head of the band, dispersing solute in both directions along the z axis under all conditions. As the ports are widened, the important dispersive mechanism will shift from crescent formation to mixing in the recycle streams. Distribution type 1 will develop a toe similar to that of type 2 and will blend into type 2 as the ports widen. But constraints 22 and 23 will remain valid, although only 22 will be of utility.

Conclusions

Detailed analysis of an ideal model of recycle continuous-flow electrophoresis has revealed useful information for construction and operation of an RCFE device. A solute's far-field concentration and direction of migration are determined by a simple expression involving the chamber dimensions, mobility, and electric field strength.

Three types of solute distribution may be found in RCFE. Separation will be easiest if operating conditions can be selected such that one solute is found only to the right of the feed, a type 1 distribution, while the other solute exhibits a rapidly decaying toe to the right of the feed, a type 3 distribution. The ability to select such conditions depends on the mobilities of the solutes being separated and the electroosmotic mobility; device dimensions play no role.

The two-sided Laplace transform proved a useful analytical tool in this problem, handily accommodating the recycle shift and nonzero far-field concentration. Inversion of the transform was straightforward (although not trivial). The two inversions are complementary, each providing information the other does not reveal.

Acknowledgment

This work was supported in part by National Science Foundation Grant No. CBT-8414218.

Notation

B = chamber half-thickness
C = concentration
C^{FF} = far-field concentration
C^* = scaled concentration
C_0 = feed concentration
D = diffusion coefficient
$D(p)$ = denominator of Laplace transform
E = electric field strength
$H(\cdot)$ = Heaviside step function
J_x, J_z = axial and lateral flux
L = chamber length
p = Laplace variable
r_n = a pole of the Laplace transform
s = shift
u_E = electrophoretic velocity
u_0 = axial centerline velocity
u_w = electroosmotic wall velocity
$U(\cdot, \cdot, \cdot)$ = Kummer function of the second kind
x, y, z = axial, transverse, and lateral coordinates

Greek letters

β = scaled measure of intensity of crescent formation
$\delta(\cdot)$ = impulse function
ϵ = scaled electrophoretic velocity
γ = scaled distance head of solute band moves in a single cycle
λ = scaled chamber length
μ = electrophoretic mobility
μ_w = electroosmotic wall mobility
ν = scaled electroosmotic wall velocity
σ = scaled shift
ξ, η, ζ = scaled axial, transverse, and lateral coordinates

Literature Cited

Abramowitz, M., and I. Stegun, *Handbook of Mathematical Functions,* Dover, New York (1964).

Barrolier, J., E. Watzke, and H. Gibian, "Simple Experimental Set-up for Carrier-Free Preparative Flow-through Electrophoresis," *Z. Naturforschung,* **13b,** 754 (1958).

Gionovario, J. A., R. N. Griffin, and E. L. Gray, "A Mathematical Model of Free-Flow Electrophoresis," *J. Chrom.,* **153,** 329 (1978).

Gobie, W. A., and C. F. Ivory, "Recycle Continuous-Flow Electrophoresis: Theory and Experiment," *AIChE Nat. Meet.,* New York (Nov., 1987b).

Gobie, W. A., J. B. Beckwith and C. F. Ivory, "High-Resolution Continuous Flow Electrophoresis," *Biotech. Prog.,* **1**(1) (1985).

Gobie, W. A., J. B. Beckwith and C. F. Ivory, "High-Resolution Continuous Flow Electrophoresis," *Biotech. Prog.,* **1**(1) (1985).

Grassmann, W., "Concerning a Procedure for the Separation of Substances by Means of Electrophoresis (According to Experiment Conducted Together with K. Hannig)," *Z. Angew. Chem.,* **62,** 170 (1950).

Grassmann, W., and K. Hannig, "Separation of Mixtures on Filtration Paper by Means of Deflection within an Electric Field," *Hoppe-Seyler's Z. Physiol. Chem.,* **292,** 32 (1953).

Hannig, K., "The Application of Free-Flow Electrophoresis to the Separation of Macromolecules and Particles of Biological Importance," *Modern Separation Methods of Macromolecules and Particles,* v. 2, T. Gerritsen, ed., Wiley, New York, **45** (1969).

———, "New Aspects in Preparative and Analytical Continuous Free-Flow Cell Electrophoresis," *Electrophoresis 1982,* **3,** 235 (1982).

Lebedev, N. N., *Special Functions and Their Applications,* R. A. Silverman, trans. and ed., Dover, New York (1972).

Mattock, P., G. G. Aitchison, and A. R. Thomson, "Velocity-Gradient Stabilized, Continuous, Free-Flow Electrophoresis. A Review," *Sep. Pur. Meth.,* **9**(1), 1 (1980).

Philpot, J. St. L., "The Use of Thin Layers in Electrophoretic Separation," *Trans. Farad. Soc.,* **36,** 38 (1940).

Saville, D. A., and S. Ostrach, "Fluid Mechanics of Continuous-Flow Electrophoresis," Final Rep., Contract NAS-8-31349, Code 361, MSFC (1978).

Strickler, A., "Continuous Particle Electrophoresis: A New Analytical and Preparative Capability," *Sep. Sci.*, **2**(3), 335 (1967).

Strickler, A., and T. Sacks, "Focusing in Continuous-Flow Electrophoresis Systems by Electrical Control of Effective Cell Wall Zeta Potential," *Ann. NY Acad. Sci.*, **209**, 497 (1973).

Svensson, H., and I. Brattsten, "An Apparatus for Continuous Electrophoretic Separation in Flowing Liquids," *Arkiv för Kemi*, **1**(47), 401, (1949).

Taylor, G., "Dispersion of Soluble Matter in Solvent Flowing Slowly through a Tube," *Proc. Roy. Soc.*, **A 219**, 186 (1953).

van der Pol, B., and H. Bremmer, *Operational Calculus Based on the Two-Sided Laplace Integral*, 2nd ed., Cambridge (1955).

Vaughn, P., "Mathematical Modeling of Continuous Particle Electrophoresis with Emphasis on Hydrodynamic Stability and Bouyancy," Ph.D. Diss., Lehigh Univ. (1983).

Yoshisato, R. A., L. M. Korndorf, G. R. Carmichael, and R. Datta, "Performance Analysis of a Continuous Rotating Annular Electrophoresis Column," *Sep. Sci.*, **21**(8), 727 (1986).

Manuscript received July 23, 1987, and revision received Nov. 30, 1987.